Construction of immunotherapy-related prognostic gene signature and small molecule drug prediction for cutaneous melanoma

Jiahua Xing
Chinese PLA General Hospital
Ziqi Jia
Chinese Academy of Medical Sciences
Yan Han (hanyanhyy10@163.com)
Chinese PLA General Hospital

Research Article

Keywords: Cutaneous melanoma, Tumor microenvironment, Prognostic signature, Immunotherapy, Bioinformatics

Posted Date: June 15th, 2022

DOI: https://doi.org/10.21203/rs.3.rs-1738111/v1

Abstract

Background

Cutaneous melanoma (CM), a kind of skin cancer with a high rate of advanced mortality, exhibits a wide variety of driver and transmitter gene alterations in the immunological tumor microenvironment (TME) associated with tumor cell survival and proliferation.

Methods

We analyzed the immunological infiltration of TME cells in normal and malignant tissues using 469 CM and 556 normal skin samples. We used a single sample gene set enrichment assay (ssGSEA) to quantify the relative abundance of 28 cells, developed a riskScore prognostic model using the LASSO COX regression model, and performed small molecule drug screening and molecular docking validation, which was finally validated using qRT-PCR and IHC.

Results

We developed a prognosis model around seven essential protective genes for the first time, dramatically elevated in tumor tissues, as did immune cell infiltration. The results of multivariate Cox regression demonstrated that riskScore is an independent and robust prognostic indicator, and its predictive usefulness in immunotherapy was verified. Additionally, we identified Gabapentin as a possible small molecule therapeutic for CM.

Conclusions

A riskScore model was developed in this work to analyze patient prognosis, TME cell infiltration features, and treatment responsiveness. The development of this model aid in predicting patient response to immunotherapy, but it also has significant implications for the development of novel immunotherapeutic agents and the promotion of tailored treatment regimens.

1. Introduction

The incidence of cutaneous melanoma (CM), a malignant tumor of the skin and mucous membranes, has been increasing globally over the past few decades. There were more than 100,000 cases of CM recorded in the United States in 2021 [1]. Although CM accounts for only 5% of all skin cancers, up to 80% of skin cancer deaths are associated with CM [2]. The incidence of CM is increasing by 3%-7% annually, posing a severe threat to human life and health [3]. Overall 10-year survival statistics for patients with early-stage CM (stages I and II) remain favorable, ranging between 75% and 94% [4]. In general, early-stage CM has a high cure rate after complete resection. In contrast, the mortality rate of patients with

advanced CM (stages III and IV) is up to 70%, and the 5-year survival rate is less than 16% [5]. CM comprises a small proportion of all skin tumors; compared to other skin tumors, CM has clinical features such as high malignancy, high recurrence rate, facile metastasis, high late mortality, and high therapeutic resistance [6] [7] [8]. Although CM has received increasing clinical attention, its clinical efficacy and patient prognosis have not reached the expected level due to its complex genetic and molecular mechanisms [9].

The treatment and management of CM has changed significantly with the advent of BRAF inhibitors, since then more and more immune checkpoint inhibitors (ICIs) have been used in treatment of CM [10] [11]. In a minority of CM patients with lasting responses, immunotherapies such as ICIs (anti-PD-1/L1 antibodies and anti-CTLA-4 antibodies) have a favorable prognosis. However, most patients do not have a favorable prognosis from them. This disparity in clinical response rates between tumors of the same and different types suggests innate and acquired immunological resistance to immune checkpoints in tumor tissue [12] [13] [14]. Numerous researchers currently believe that the tumor microenvironment (TME) comprises a network of tumor cells and stromal cells (fibroblasts, vascular cells, and inflammatory immune cells), which play a crucial role in immune evasion and immunotherapy resistance [15]. Therefore, this study utilized immune-related gene sets in conjunction with clinical data from many databases to build a prediction model with TME immune cell infiltration features as its core, then verified it with multi-omics. In addition, for the first time, this study employs highly expressed tumor-protective genes as the core of the model and small molecule therapeutic screening and molecular docking validation.

2. Material And Method

2.1 Gene expression profiles of CM and normal skin tissue

We first downloaded the TCGA TARGET GTEx dataset from the UCSC database (https://xena.ucsc.edu/) and extracted the normal group in TCGA and the normal skin data in GTEx as the control group. Our study included 1025 CM expression profile cohorts, including the TCGA and GTEx. We downloaded the COUNT gene expression values from public genomic data using the R package TCGAbiolinks [16]. 469 CM samples and 556 normal samples were obtained for this study. We utilized the R package Combat algorithm to correct for batch effects due to abiotic bias. In addition, we downloaded immune-related genes from the Immport (https://www.immp ort.orgc) database for subsequent analysis.

2.2 Screening of immune-related differentially expressed genes (DEGs)

To identify key molecules associated with patients' prognosis and TME cellular immune infiltration characteristics, we identified differentially expressed genes (DEGs) in CM and normal skin tissue using the empirical Bayes method in the R language limma-voom package. We used $P < 0.01$ and $|\log FC| \geq 2$ as a cut-off criterion to screen significantly DEGs. In addition, we utilized the R package ClusterProfiler for gene ontology (GO) and Kyoto Encyclopedia of Genes and Genomes (KEGG) enrichment analysis to investigate further the potential biological processes related to immune-related DEGs [16].

2.3 Multi-omics analysis to identify key molecules

First, we submitted all DEGs to the STRING database to generate network maps of their protein-to-protein interactions (PPI). Then, we identify significant sub-network modules from the PPI network using the MCODE plugin for Cytoscape. We established the cutoff criterion as follows: degree cutoff = 10, node score cutoff = 0.2, k-core = 2, max.depth = 100. We will choose genes with high connection and significant predictive value ($P < 0.01$) among significant subnetwork modules as important molecules [17]. Finally, we chose CD86, CXCL9, FCGR3A, GZMB, PRF1, STAT1, and TLR7 as our key molecules. We utilized TCGA mutation data to show key molecules' mutation frequencies and mutation types in CM patients. 467 CM patients with complete clinical annotation were available for CM survival analysis. We utilized the R package survminer to determine appropriate cut-off points, categorized patients into high- and low-risk groups and employed the Human Protein Atlas (https://www.prote inatlas.org/) database to evaluate the protein expression of key molecules between CM and normal skin tissue.

2.4 Extrapolation of TME infiltrating cells

We utilized single sample gene set enrichment analysis (ssGSEA) to estimate the infiltration abundance of each TME cell based on the Cibersort gene set [18]. We accommodated the enrichment scores for each TME cell subtype using the ESTIMATE algorithm to control the bias caused by tumor purity [19]. We employed 28 human TME cell subtypes and expressed the abundance of each TME-infiltrating cell by the adjusted enrichment scores determined using ssGSEA.

2.5 Construction of a key molecules-based prognostic model

We constructed riskScore models based on the involvement of these seven critical genes in the course of CM in order to analyze the relevance of these molecules in patient prognosis, TME immune cell infiltration, and immunotherapy responsiveness. We created prognostic models for fitting the overall survival (OS) of CM patients using least absolute shrinkage and selection operator (LASSO) Cox regression analysis. In order to construct the optimal prognostic model, we utilized the R language's glmnet package to select and reduce the variables so that some of the regression coefficients were strictly equal to 0. In addition, we employ 10 cross-validations to establish the penalty parameter (λ) of the prognostic model and adhere to the minimum criterion (the value of λ corresponds to the lowest likelihood deviation) [20]. The riskScore is defined as riskScore= $\sum_{i=1}^{n} Coefficient \times Expression$. The coefficient is defined as the coefficient derived using LASSO COX regression, and Expression is defined as the expression of important genes.

2.6 Access to Immunotherapy Cohort and Clinical Information

We included in our analysis the IMvigor210 immunotherapy group from prior studies with complete clinical and transcriptome data [21]. The IMvigor210 cohort focuses on the efficacy of an anti-PD-L1 antibody (pembrolizumab) in patients with advanced uroepithelial carcinoma. IMvigor210 cohort has been widely used in lung adenocarcinoma [22], colon cancer [23], breast cancer [24], hepatocellular

carcinoma [25], and head and neck squamous cell carcinoma [26] as a high-quality and comprehensive immunotherapy cohort to evaluate the predictive effect of immunotherapy in different types of tumor prediction models. We downloaded the complete transcriptomic data and detailed clinical information from the relevant URL (http://research-pub.gene.com/ IMvigor210CoreBiologies/). Then, using the R package DEseq2, we normalized the data and transformed the count values to TPM values.

2.7 Chemotherapy drug sensitivity analysis, small molecule drug screening and molecular docking validation

First, we utilized the R package pRRophetic to examine the half-maximal inhibitory concentrations (IC50) of common chemotherapeutic agents and targeted medicines to quantify our riskScore model's prediction power for CM treatment. After that, Using the Cmap (Connectivity Map) database, we calculated medications having significantly negative correlations with seven highly elevated genes and then picked the top 10 drugs [27]. Then, we obtained the SDF 2D structure files of the 10 drug candidates from the Pubchem database, transformed the small molecules into 3D structure files using Autodock MGLTools, performed energy optimization, and then exported the files in PDBQT format. We downloaded seven highly up-regulated genes from the PDB database to determine crystal structures. However, CXCL9 and PRF1 were excluded from the subsequent molecular docking investigation because they lacked crystal structure information. The receptor crystal structures were processed in bulk using the prepare_recpetor4.py script in Autodock MGLTools, then docked to small molecules and receptor proteins using Autodock Vina (version 1.1.2). We used Pymol to map the small molecule-protein binding and visualize molecular docking results [28]. The docking scoring heat map was generated using the R package ComplexHeatmap.

2.8 Validation of key molecules in cells and tissues

We utilized the following cell lines to validate key genes in CM and normal skin tissues. We employed the A375 human melanoma cell line, SK-MEL-28 human melanoma cell line, human immortalized keratin-forming cell line (Hacat), and human melanocyte cell line (PIG1) in this study. All cells were grown in RPMI-1640 media supplemented with 10% fetal bovine serum in a 37°C, 5% CO_2 atmosphere.

Then, we collected 20 fresh frozen CM tumor tissue and normal skin tissue specimens, each for self-matching and divided them into tumor group and normal group. The specimens and patients were in one-to-one correspondence. The Human Research Ethics Committee of the Chinese PLA General Hospital authorized all experimental components, and patients signed informed permission forms. We utilized qRT-PCR to detect the relative expression of seven key genes in fresh frozen specimens. Using Trizol reagent, we extracted total RNA from the four cell lines and tissues listed above. RNA concentration was determined using a NanoDrop spectrophotometer. We synthesized cDNA using PrimerScript 5×RT Master Mix (BioRad), and mRNA expression levels were quantified using a 2×SYBR Green PCR Kit based on fresh frozen specimens. The mRNA expression level of each gene was normalized by GAPDH (glyceraldehyde-3-phosphate dehydrogenase) that was used as the internal reference. Utilizing the $2^{-\Delta\Delta Ct}$ approach, we

quantified the real-time PCR analysis and determined the relative expression of essential genes individually in cells and human specimen tissues. Beijing Huada Corporation produced all primers. We presented the primer sequences and patient specimens' information in the Supplemental Table 1–2. In addition, we downloaded immunohistochemical (IHC) images of key genes' CM and normal skin tissue from the Human Protein Atlas database. We selected a suitable field of view in each IHC image of normal skin tissues and CM for semi-quantitative analysis of protein expression levels using Image Pro Plus 6.0.

2.9 Statistical analysis

We utilized the Wilcoxon test to analyze the differences between the two groups in this study. In comparison, one-way ANOVA and the Kruskal-Wallis test were employed to determine the significance of differences among three or more groups. Spearman's analysis was used for correlation testing. We utilized univariate Cox regression models to construct hazard ratios (HR) and 95 percent confidence intervals (95%CI), and multivariate Cox model models to investigate the predictive potential of riskScore as an independent prognostic biomarker for assessing patient prognosis. All statistical *P* values in this investigation were two-tailed, and $P < 0.05$ was considered statistically significant.

3. Results

3.1 Genomic mapping differences between normal and CM

The study's flowchart is depicted in Supplementary Fig. 1. Using cluster analysis and principal component analysis (PCA), we first demonstrated the genetic differences between normal skin tissues and CM (Fig. 1A-B). By comparing 469 CM and 556 normal skin tissues, we discovered that the expression of 4555 genes was significantly altered in tumor tissues against normal tissues ($P < 0.01$, $|\log FC| \geq 2$), with 2296 genes considerably up-regulated and 2259 genes significantly down-regulated (Fig. 1C). The GO enrichment analysis demonstrates that CM genetic variants play a role in TME immune components and matrix-related biological processes, such as cytokine-mediated signaling pathway, cell chemotaxis, and positive regulation of response to external stimulation (Fig. 1D-G). The KEGG pathway indicates that these genes are also involved in immune-related signaling pathways, such as cytokine-cytokine receptor interaction, viral protein interaction with the cytokine-cytokine receptor, viral protein interaction with cytokine and cytokine receptor, and natural killer cell-mediated cytotoxicity (Fig. 1H). The heatmap results also imply that immunological and matrix-related pathways play a significant role in the CM genome (Fig. 1I). The PPI network reveals a close interaction between CM-related genes at the protein level (Fig. 2A). We identified a sub-network module with solid predictive value, in which CD86, CXCL9, FCGR3A, GZMB, PRF1, STAT1, and TLR7 were designated as key molecules with high connectedness. We also investigated the protein correlation between these key molecules (Fig. 2B-C). We found that the expression of critical molecules is significantly elevated in CM samples relative to normal samples (Fig. 2D). We performed dimensionality reduction using PCA to determine if these critical molecules can distinguish CM samples from normal samples. We discovered two completely disjoint populations, indicating that the expression patterns of critical molecules in normal and CM samples are distinct

(Fig. 2E). In addition, we demonstrated the interaction of numerous immune molecules in the CM TME, the signaling cascade and transmission, and the distinct regulation patterns between molecules (Fig. 2F).

3.2 Multi-omics analysis to identify key molecules and mutation and survival analysis

We obtained immunohistochemistry results for seven critical molecules from the HPA database and qualitatively found protein-level expression variations between normal tissues and CM samples (Fig. 3A-B). In a subsequent confirmation, we evaluated the expression of these important molecules in cell lines and 20 pairs of tumors and surrounding normal tissues to validate the differential and significant expression of essential molecules in CM tissues. Spearman correlation analysis identified a significant positive correlation between important molecules and a strong interaction between these molecules (Fig. 3C). The mutations of CM's essential molecules were then studied. Among the 467 patients with complete clinical annotation information, 72 patients (15.42%) had mutations in at least one gene locus. CD86 had the highest frequency of mutations in CM samples, followed by TLR7, and all essential molecules were found with gene mutation (Fig. 3D). The expression and mutation of these essential molecules may play a crucial role in the growth and metastasis of CM, as deduced by our findings. In addition, we probed into the predictive value of key molecules based on an independent CM cohort from the TCGA database using survival analysis. The TCGA-CM cohort also demonstrated variations in the expression of essential molecules between normal and tumor samples. For survival analysis, 467 CM patients with complete clinical annotation were available. Patients with high expression of CD86, CXCL9, FCGR3A, GZMB, PRF1, STAT1, and TLR7 had a significant survival benefit over those with low expression (Fig. 4A-G). Seven critical molecules displayed significantly greater expression levels in CM, and all seven key molecules as protective molecules significantly increased CM patient survival.

3.3 Evaluation of immune cell infiltration characteristics of tumor microenvironment

To further investigate the role of identified critical molecules in TME immune cell infiltration in CM patients, we analyzed the infiltration of 28 types of TME cells in normal and tumor tissues (Fig. 5A). T helper cells (type 1 and 2), activated B cells, $CD4^+$ T cells, $CD8^+$ T cells, immature B cells, regulatory T cells, natural killer cell, activated dendritic cell, plasmacytoid dendritic cell, MDSC, monocyte, memory B cell, macrophage, gamma delta T cell, effector memory $CD4^+$ T cells, CD56 dim natural killer cell, immature dendritic cell, eosinophil, $CD8^+$ T cells were highly plentiful in tumor tissue. However, other cell subsets were notably abundant in normal tissue. Then, using the PCA algorithm, we compared the infiltration patterns of TME cells in normal and tumor tissues to determine if there were any differences. After dimensionality reduction, the results demonstrated the existence of two distinct populations of TME cells (Fig. 5B). Using the ESTIMATE algorithm, we determined the immunological and mesenchymal activity in the CM microenvironment. It was discovered that immune and mesenchymal activities were much higher in tumor tissues than normal skin tissues (Fig. 5C-D). To examine the link between critical molecules and immune cells in the TME, we correlated key molecules with cellular fractions in the TME. Spearman correlation analysis revealed that these molecules were strongly positively linked with most TME cellular fractions, except T helper cells, CD56 bright natural killer cells, and neutrophil cell infiltration

(Fig. 5E). In addition, the expression of seven essential molecules demonstrated a significant positive association with PD-L2 and PD-L1 and a negative correlation with CTLA4 (Fig. 5F). CTLA4 had the most significant connection with STAT1 and TLR7 (Fig. 5G-H).

3.4 Correlation model construction for prognosis and immunotherapy based on key molecules

We incorporated patient prognostic information and TME immune cell infiltration status to build the riskScore model, and we integrated the role of these essential molecules using LASSO Cox regression. RiskScore was determined by the expression of the four most representative important molecules, according to the findings (Fig. 6A-B). Based on the critical value of -7.07 (Fig. 6C) computed by the MaxStat R package, we classified the patients into high-risk and low-risk groups. We observed that the low-risk group had a considerable survival advantage over the high-risk group (Fig. 6D). In addition, the expression of these essential molecules is much higher in low-risk tumors than in high-risk, suggesting that these key molecules have a protective role in the low-risk group, consistent with the findings of our earlier investigation (Fig. 6E-F). With rising risk, patient mortality might climb significantly (Fig. 6G-H). Our examination of multivariate COX regression models incorporating basic clinical and pathological information about the patients demonstrated that riskScore could be an independent and robust predictive biomarker to evaluate CM patients (Fig. 7A). In addition, we developed a nomogram that combines the riskScore with independent clinical prognostic indicators to estimate the likelihood of patient mortality (Fig. 7B). The calibration plots demonstrated that the generated nomogram had a superior prediction ability (Fig. 7C). We displayed ROC curves based on TCGA data with AUC of 0.757, 0.675, and 0.657 for 1, 2, and 3 years, indicating the riskScore's predictive performance is acceptable and can provide a reference for clinical decision-making (Fig. 7D). In addition, our findings demonstrated that riskScore surpassed other clinical factors, such as age and number of nodules, in predicting OS in patients with CM (Fig. 7E).

We utilized gene set enrichment analysis (GSEA) to investigate the activated biological pathways in the low-risk and high-risk groups. Compared to the low-risk group, cancer-related pathways such as P53, PI3K-AKT-mTOR, NOTCH, and WNT were considerably activated in the high-risk group (Fig. 7F-K). Then we analyzed the difference in TME cell infiltration between the low-risk and high-risk groups, and we discovered that all immune infiltrating cells, except for CD56 dim natural killer cells and CD56 bright natural killer cells, were significantly higher in the low-risk group than in the high-risk group (Fig. 8A). By correlation analysis, we discovered that riskScore values were strongly and positively linked with the majority of TME cell infiltrating rates (Fig. 8B). We also discovered a significant and positive correlation between riskScore values and the expression of immune checkpoint molecules, indicating the potential predictive role of riskScore in predicting clinical response to immunotherapy and providing a foundation for developing novel immunotherapies (Fig. 8C). As immune checkpoint blockade (ICB) has made advances in the treatment of CM over the past few years, we verified riskScore's ability to predict the clinical response of patients to ICB therapy. In the IMvigor210 cohort treated with anti-PD-L1 therapy, low-risk patients had a considerable clinical benefit and prolonged survival (Fig. 8D). The patients with

complete remission (CR) or stable disease (SD) had a lower risk (Fig. 8E). In addition, we noticed that low-risk individuals responded considerably better to PD-L1 blocking therapy than high-risk patients (Fig. 8F).

3.5 Chemotherapy drug sensitivity analysis, small molecule drug screening and molecular docking validation

We analyzed 20 common chemotherapeutic and targeted medicines and found substantial variations between the high-risk and low-risk categories in IC50 values (Supplementary Fig. 2). The results indicate that our riskScore signature can uncover prospective biomarkers of chemotherapy and targeted medication sensitivity. Then, we calculated the connection between medication-treated expression profiles and highly up-regulated expression profiles of seven key genes using the Cmap database. We then identified the top ten pharmaceuticals with negative correlations as potential treatment candidates (Table 1). Figure 9A-J shows the chemical structures of these ten compounds. AGI-6780 and Zofenopril-calcium bind well to GZMB, indicating that these two small compounds can be employed as possible target medicines to target GZMB. In addition, we utilized Pymol to generate a heatmap of the binding of CD86, FCGR3A, STAT1, TLR7, and GZMB proteins to the most strongly bound small molecules or the top two most strongly bound small molecules (Fig. 9K). The results demonstrated that the small molecules of CD86 bound to Baricitinib formed hydrogen bonds with THR-69, SER-67, GLN-16. The binding of FCGR3A to Zofenopril-calcium formed hydrogen bonds with HIS-111 and ARG-109. The binding of GZMB to Zofenopril-calcium formed hydrogen bonds with LYS-113 and ARG-87, and no hydrogen bonds were formed in the binding of AGI-6780. Small molecules in the binding of STAT1 to Calcipotriol formed hydrogen bonds with GLU-353 and GLN-271, and small molecules in the binding of TLR7 to Zofenopril-calcium formed hydrogen bonds mainly with LYS-464. The majority of receptor and ligand binding energies are less than − 7 $kcal.mol^{-1}$, indicating that the target protein and active ingredient can bind spontaneously with high affinity and stable conformation, and thus small molecule medicines are likely to act on these targets. To illustrate the molecular interactions, we chose the small molecule medication with the lowest binding energy to dock the target for docking visualization (Fig. 10A-H).

Table 1
Results of Cmap analysis

Cmap name	N	Celline	Enrichment	FDR_Q_nlog10
Gabapentin	2	YAPC	-0.94	15.65
Baricitinib	3	HBL1	-0.92	15.65
DPN	3	A549	-0.91	15.65
AGI-6780	2	PC3	-0.9	15.65
Fusaric-acid	3	SKB	-0.9	15.65
Ru-24969	3	MCF7	-0.89	15.65
Calcipotriol	2	HCC515	-0.89	15.65
Fenoterol	2	YAPC	0.89	15.65
Zofenopril-calcium	2	JURKAT	-0.89	15.65
RS-102895	3	A549	-0.89	15.65

3.6 Expression validation of key molecules

We validated the differential expression of these proteins in normal skin tissues and CM using semi-quantitative analysis after selecting one appropriate field of view (the first column of Fig. 11). qRT-PCR was subsequently utilized to confirm the differential expression of these seven essential genes in cell lines and human specimens. The mRNA expression of seven key genes was considerably higher in the A375 and SK-Mel-14 cell lines than in the Hacat and PIG1 cell lines. (the second column of Fig. 11). Similarly, we discovered that the patients' mRNA expression of seven key genes was much higher in CM than in normal skin tissue (the third column of Fig. 11). Using experimental validation at the mRNA and protein levels, we determined that CD86, CXCL9, FCGR3A, GZMB, PRF1, STAT1, and TLR7 were differentially expressed in normal skin tissues and CM and inferred that these key molecules could be potentially critical targets for the treatment of CM.

4. Discussion

In recent years, chemotherapy, immunotherapy, and targeted therapies have been utilized to treat patients with advanced CM. Nonetheless, there are still issues such as high drug resistance, low drug sensitivity, and poor prognosis. Substantial advancements in sequencing technologies have created new options for methodically deciphering key genes and epigenetic alterations in various kinds of CM. In this study, we combined immune-related gene sets and other datasets to explore the complex integrative roles of multiple key molecules on TME infiltration and heterogeneity. We not only revealed the potential

mechanisms of TME anti-tumor immune response, but also screened potential biological therapeutic targets and performed small molecular drugs prediction.

Numerous CM prognostic models created based on different aspects have shown distinct therapeutic applicability in recent years. However, few CM models are available for immune genes, immunotherapy, and small molecule drug prediction. Zhang et al. established a five-mRNA prognostic signature to predict CM prognosis and immunotherapy response [29]. Wu et al. created a four pyroptosis genes-associated prognosis signature predicted the 1-year OS of CM with AUC of 0.705 and 0.582 for the training and validation sets, respectively [30]. Our time-dependent ROC curve predicted the 1-year OS of CM patients with an AUC of 0.757, which was superior to these signatures. We also compared other recent CM prognostic signatures constructed from different perspectives [31] [32] [33], and we found that the prognostic signature in this study showed better clinical predictive performance in comparison.

We investigated the key molecules affecting patient prognosis in the present study using 469 CM samples and 556 normal skin samples with multiple database gene sets. By studying the genetic changes between normal skin tissues and CM tissues, we discovered that immune-related pathways exhibited significant differences. We employed seven key molecules with high interaction as the foundation of the prediction model. The expression of these seven essential genes was dramatically elevated in tumor tissue as protective genes and was highly correlated with a significantly more extended survival period. Through immune-related analysis, we determined that CM had much higher immune cell infiltration levels than normal skin and significantly higher total immunological and mesenchymal activity, which altered the TME's infiltration pattern. We used the LASSO COX regression model to develop the riskScore signature. We discovered that low-risk patients had more significant TME immune cell infiltration and a longer survival time. We also discovered that riskScore could be utilized as an independent biomarker to assess patient prognosis by multivariate COX regression. We integrated riskScore and independent clinical prognostic markers to generate nomogram plots that displayed excellent predictive performance. In the IMvigor210 group receiving anti-PD-L1 therapy, we observed a significant therapeutic benefit with increased survival time and enhanced clinical response in low-risk patients compared to those at high risk, which demonstrates the good predictive performance of our riskScore signature. Moreover, using small molecule drug screening and molecular docking, Gabapentin and Baricitinib were discovered as prospective small-molecule medicines to treat CM. Finally, we utilized IHC and qRT-PCR to confirm the expression of important molecules.

CM is considered one of the most immunogenic tumors due to its high mutational load, and many immune cells infiltrate. Immune cell infiltration is an essential protective mechanism of the organism and forms the basis for overt cellular therapies and cellular vaccines to treat cancer. All seven genes in our riskScore signature are mutated in CM patients, with the highest frequency of mutations in CD86. Studies have shown that CD86 gene polymorphisms in miRNA are associated with the risk of malignancies such as pancreatic, cervical, and colon cancers. Therefore, we speculate that CD86 may be one of the potential targets for CM therapy [34]. The riskScore signature consists of seven key molecules, CD86, CXCL9, FCGR3A, GZMB, PRF1, STAT1, and TLR7, all of which are expressed up-regulated in CM as protective

molecules. CD86 (cluster of differentiation 86), a member of the immunoglobulin superfamily, interacts with the inducer CD28 and the inhibitor CTLA4 and functions as a crucial cofactor in the stimulation of T-lymphocyte proliferation and IL-2 production [35]. CTLA4, an immunological checkpoint molecule, can influence the TME of CM by binding to B7 (CD80/CD86) molecules on melanoma antigen-presenting cells to down-regulate T cell activation [36]. The chemokine CXCL9 (C-X-C motif chemokine ligand 9) correlates positively with $CD8^+$T cell infiltration in solid malignancies [37] [38]. CXCL9 is abundantly expressed in several solid tumors, including CM, and it stimulates the infiltration of $CD4^+$T and $CD8^+$T lymphocytes into tumor cell regions, so boosting the response of cytotoxic T lymphocytes and thereby killing tumor cells [39] [40]. FCGR3A (Fc fragment of IgG receptor IIIa) encodes the receptor for the Fc region of immunoglobulin G. FCGR3A interacts with FCGR1A in numerous pathophysiological processes and is substantially related with overall survival (OS) in CM, renal clear cell carcinoma, and other malignancies [41]. Granzyme B (GZMB) is an exogenous serine protease generated from granules released by cytotoxic lymphocytes (CTLs) and natural killer cells (NK) [42]. GZMB has been discovered to be related with NK cell treatment in individuals with CM. By evaluating NK cells in the blood of CM patients, it was discovered that NK cells entering metastatic melanoma tissue have a diminished cytotoxic capacity due to decreased expression of GZMB and perforin [43]. PRF1 (perforin 1) encodes a protein structurally similar to complement C9, which plays a crucial function in immunity [44]. Tumors of CM patients treated with the anti-PD1 medication nivolumab demonstrated dramatically higher levels of PRF1, CD8, and GZMA, as well as an enhanced TBX21/GATA3 ratio, according to research. This suggests that PRF1 mediates tumor-infiltrating T lymphocytes (TIL) oligoclonal amplification-enhanced Th1 (helper T cell type I)-skewed cellular immunity during nivolumab treatment [45]. STAT1 (signal transducers and activators of transcription 1) is a family of cytosolic proteins that, upon activation, can translocate to the nucleus and bind DNA, which has dual signal transduction and transcriptional control functions [46] [47]. Hypermethylation in the promoter region of the SOCS3 gene was discovered to reduce SOCS3 protein expression in some CM patients. The greater the sensitivity of melanoma cells to IFN-γ, the lower the expression of SOCS3, and the lowering of SOCS3 expression in melanoma cells by IFN-γ may significantly stimulate the production of STAT1 [48]. TLR7 (toll-like receptors 7) is an endosomal pattern recognition receptor, when activated, causes type I interferons and inflammatory reactions [49]. TLR7 plays a crucial role in activating both natural and acquired immune responses and has an activating effect on virtually all cells engaged in the tumor immune response [50]. It was discovered that chemically coupling ibrutinib with TLR7 receptor agonists to produce novel immune-targeting complexes called GY161 increased the levels of $CD8^+$T cells in spleen and tumor in vivo. GY161 inhibited the growth of B16 melanoma cell-derived tumors and prolonged the survival time of mice [51].

The significance of the TME in tumor development is critical. Numerous studies have demonstrated that different immune cells can operate as tumor promoters or tumor antagonists in various tumors [52] [53]. Therefore, it is necessary to do additional research on immune infiltration in TME better to comprehend the relationship between immune components and tumor progression. After constructing a riskScore model to divide the high- and low-risk groups, we discovered that the expression of seven protective key molecules was significantly lower in the high-risk group. In contrast, immune cell infiltration was

significantly lower in the high-risk group compared to the low-risk group. We discovered that the group at low risk had more extensive levels of $CD4^+$ and $CD8^+$ T cells. $CD8^+$ T cells eliminate tumor cells based on cell differentiation and invasion. They can differentiate into effector and cytotoxic T cells to perform anti-tumor actions in the tumor-infiltrating microenvironment [54]. In secondary lymphoid organs, $CD4^+$ T cells can inhibit or stimulate the activity of anti-tumor cytotoxic T cells, hence modulating tumor cells. Tumor infiltration lymphocytes (TILs) in CM are a potential immunotherapy target in the future [55]. Inflammation also plays a vital role in TME and tumor formation. Since Virchow proposed in 1863 that tumor formation originates from chronic inflammation, numerous studies have confirmed that some tumors are closely associated with chronic inflammation. We found significantly more inflammation-associated immune cell infiltration in CM than in normal skin, suggesting a pro-tumor effect of inflammation in the TME. It can assist the proliferation and survival of cancer cells as well as promote angiogenesis and metastasis [56]. Our riskScore signature demonstrated significantly higher inflammation-associated immune cell infiltration in the low-risk group compared to the high-risk group. The low-risk group had higher MDSCs, TILs ($CD4^+$ T cells and $CD8^+$ T cells), TAMs, dendritic cells, neutrophils, and mast cells. MDSCs are immature bone marrow cells that suppress natural and adaptive immunity and evade immune surveillance [57]. TAMs can mainly promote tumor growth and increase vascular growth and invasive metastasis [58]. Neutrophils and TILs can play a role in killing tumor cells. B lymphocytes and mast cells also play an essential role in immune-mediated tumor growth. In additional, macrophages and dendritic cells play antigen presentation and T-cell activation roles and have immunosuppressive functions in tumors [59].

The innovative use of traditional drugs has now become an important strategy for antineoplastic drug development. The discovery of potential mechanisms of conventional medications can save time and money while also enhancing the security of drug administration. Gabapentin and Baricitinib promise medications for the treatment of CM, per the CMAP database. Gabapentin, whose mechanism of action is currently unknown, is commonly believed to modify the GABA metabolic pathway in patients with circumscribed seizures that are not adequately controlled or tolerated by traditional antiepileptic medicines. Several investigations have verified the anticancer effects of Gabapentin in recent years. Gabapentin may achieve anti-melanoma effects in mice by reducing cell proliferation, CCL2 production, and calcium influx [60]. In recent years, it has been demonstrated that thiamine-dependent enzymes (TDEs) are frequently tumor-related targets due to their control of metabolic pathways that are frequently altered in cancer. Gabapentin can impede the growth of TDEs, resulting in a tumor-killing mechanism of toxicity [61]. Through molecular docking analysis and the summary of key molecules mentioned above, we found that Gabapentin most likely acts through STAT1 and TLR7 to achieve anti-tumor effects by altering the immune infiltration content of TILs such as $CD8^+$ T cells in TME to inhibit the proliferation and invasion of CM cells.

There are some limitations to this study. First, the clinical parameters integrated with this study may not be comprehensive due to the limited clinical information in the public dataset, leading to potential bias in our construction of the riskScore signature. Second, the plasticity of immune cells or other disease-

induced cellular changes may bias the analysis results. In addition, we constructed the riskScore signature mainly based on the TCGA database. Considering the different compatibility of different databases, we should be cautious when using this study's riskScore signature for testing in other databases.

In conclusion, the riskScore signature developed in this study can be utilized as an independent and reliable biomarker to predict the prognosis of individuals with CM. In addition, we screened and predicted small-molecule pharmaceuticals. This study not only provides riskScore signature that can predict patient prognosis and assess the heterogeneity and complexity of TME cell infiltration, but it also contributes to the development and guidance of novel immune combination therapy strategies and the promotion of the development of personalized tumor immunotherapy and precision medicine.

Declarations

Ethics approval and consent to participate:

Following permission from the Chinese PLA General Hospital's Human Research Ethics Committee, we collected twenty pairs of CM and para-cancerous normal tissue specimens. Written informed consent was obtained from individual or guardian participants.

Consent for publication

Not applicable.

Availability of data and material

All data generated or analyzed during this study are included in this published article and its supplementary files.

Competing interests

The authors declare that they have no competing interests.

Funding

Not applicable.

Authors' contributions

Jiahua Xing performed the most contributions to research design and data analysis. *Ziqi Jia* designed the study, *Yan Han* suggested ideas and participated in the revision of the manuscript. All authors contributed to the article and approved the submitted version.

Acknowledgements

Not applicable.

References

1. R.L. Siegel, K.D. Miller, H.E. Fuchs, A. Jemal, Cancer Statistics, 2021, CA: a cancer journal for clinicians, 71 (2021) 7–33.
2. R.E. Hunger, S.M. Seyed Jafari, S. Angermeier, M. Shafighi, Excision of fascia in melanoma thicker than 2 mm: no evidence for improved clinical outcome, The British journal of dermatology, 171 (2014) 1391–1396.
3. S. Felton, R.S. Taylor, D. Srivastava, Excision Margins for Melanoma In Situ on the Head and Neck, Dermatologic surgery: official publication for American Society for Dermatologic Surgery [et al.], 42 (2016) 327–334.
4. R.A. Scolyer, R.V. Rawson, J.E. Gershenwald, P.M. Ferguson, V.G. Prieto, Melanoma pathology reporting and staging, Modern pathology: an official journal of the United States and Canadian Academy of Pathology, Inc, 33 (2020) 15–24.
5. L.E. Haydu, S.N. Lo, J.L. McQuade, R.N. Amaria, J. Wargo, M.I. Ross, J.N. Cormier, A. Lucci, J.E. Lee, S.D. Ferguson, R.P.M. Saw, A.J. Spillane, K.F. Shannon, J.R. Stretch, P. Hwu, S.P. Patel, A. Diab, M.K.K. Wong, I.C. Glitza Oliva, H. Tawbi, M.S. Carlino, A.M. Menzies, G.V. Long, A.J. Lazar, M.T. Tetzlaff, R.A. Scolyer, J.E. Gershenwald, J.F. Thompson, M.A. Davies, Cumulative Incidence and Predictors of CNS Metastasis for Patients With American Joint Committee on Cancer 8th Edition Stage III Melanoma, Journal of clinical oncology: official journal of the American Society of Clinical Oncology, 38 (2020) 1429–1441.
6. M. Matias, J.O. Pinho, M.J. Penetra, G. Campos, C.P. Reis, M.M. Gaspar, The Challenging Melanoma Landscape: From Early Drug Discovery to Clinical Approval, Cells, 10 (2021).
7. L. Yang, Y. Xu, Y. Yan, P. Luo, S. Chen, B. Zheng, W. Yan, Y. Chen, C. Wang, Common Nevus and Skin Cutaneous Melanoma: Prognostic Genes Identified by Gene Co-Expression Network Analysis, Genes, 10 (2019).
8. C. Karimkhani, A.C. Green, T. Nijsten, M.A. Weinstock, R.P. Dellavalle, M. Naghavi, C. Fitzmaurice, The global burden of melanoma: results from the Global Burden of Disease Study 2015, The British journal of dermatology, 177 (2017) 134–140.
9. R.G. Witt, D.J. Erstad, J.A. Wargo, Neoadjuvant therapy for melanoma: rationale for neoadjuvant therapy and pivotal clinical trials, Therapeutic advances in medical oncology, 14 (2022) 17588359221083052.
10. J.R. Dixon-Douglas, R.P. Patel, P.M. Somasundram, G.A. McArthur, Triplet Therapy in Melanoma - Combined BRAF/MEK Inhibitors and Anti-PD-(L)1 Antibodies, Current oncology reports, (2022).
11. P.F. Ferrucci, M. Lens, E. Cocorocchio, Combined BRAF-Targeted Therapy with Immunotherapy in BRAF-Mutated Advanced Melanoma Patients, Current oncology reports, 23 (2021) 138.

12. H.R. Ali, L. Chlon, P.D. Pharoah, F. Markowetz, C. Caldas, Patterns of Immune Infiltration in Breast Cancer and Their Clinical Implications: A Gene-Expression-Based Retrospective Study, PLoS medicine, 13 (2016) e1002194.
13. A.M. Newman, C.L. Liu, M.R. Green, A.J. Gentles, W. Feng, Y. Xu, C.D. Hoang, M. Diehn, A.A. Alizadeh, Robust enumeration of cell subsets from tissue expression profiles, Nature methods, 12 (2015) 453–457.
14. M. Angelova, P. Charoentong, H. Hackl, M.L. Fischer, R. Snajder, A.M. Krogsdam, M.J. Waldner, G. Bindea, B. Mlecnik, J. Galon, Z. Trajanoski, Characterization of the immunophenotypes and antigenomes of colorectal cancers reveals distinct tumor escape mechanisms and novel targets for immunotherapy, Genome biology, 16 (2015) 64.
15. F.R. Greten, S.I. Grivennikov, Inflammation and Cancer: Triggers, Mechanisms, and Consequences, Immunity, 51 (2019) 27–41.
16. M.E. Ritchie, B. Phipson, D. Wu, Y. Hu, C.W. Law, W. Shi, G.K. Smyth, limma powers differential expression analyses for RNA-sequencing and microarray studies, Nucleic acids research, 43 (2015) e47.
17. W.P. Bandettini, P. Kellman, C. Mancini, O.J. Booker, S. Vasu, S.W. Leung, J.R. Wilson, S.M. Shanbhag, M.Y. Chen, A.E. Arai, MultiContrast Delayed Enhancement (MCODE) improves detection of subendocardial myocardial infarction by late gadolinium enhancement cardiovascular magnetic resonance: a clinical validation study, Journal of cardiovascular magnetic resonance: official journal of the Society for Cardiovascular Magnetic Resonance, 14 (2012) 83.
18. D.A. Barbie, P. Tamayo, J.S. Boehm, S.Y. Kim, S.E. Moody, I.F. Dunn, A.C. Schinzel, P. Sandy, E. Meylan, C. Scholl, S. Fröhling, E.M. Chan, M.L. Sos, K. Michel, C. Mermel, S.J. Silver, B.A. Weir, J.H. Reiling, Q. Sheng, P.B. Gupta, R.C. Wadlow, H. Le, S. Hoersch, B.S. Wittner, S. Ramaswamy, D.M. Livingston, D.M. Sabatini, M. Meyerson, R.K. Thomas, E.S. Lander, J.P. Mesirov, D.E. Root, D.G. Gilliland, T. Jacks, W.C. Hahn, Systematic RNA interference reveals that oncogenic KRAS-driven cancers require TBK1, Nature, 462 (2009) 108–112.
19. K. Yoshihara, M. Shahmoradgoli, E. Martínez, R. Vegesna, H. Kim, W. Torres-Garcia, V. Treviño, H. Shen, P.W. Laird, D.A. Levine, S.L. Carter, G. Getz, K. Stemke-Hale, G.B. Mills, R.G. Verhaak, Inferring tumour purity and stromal and immune cell admixture from expression data, Nature communications, 4 (2013) 2612.
20. J. Gao, P.W. Kwan, D. Shi, Sparse kernel learning with LASSO and Bayesian inference algorithm, Neural networks: the official journal of the International Neural Network Society, 23 (2010) 257–264.
21. S. Mariathasan, S.J. Turley, D. Nickles, A. Castiglioni, K. Yuen, Y. Wang, E.E. Kadel, III, H. Koeppen, J.L. Astarita, R. Cubas, S. Jhunjhunwala, R. Banchereau, Y. Yang, Y. Guan, C. Chalouni, J. Ziai, Y. Şenbabaoğlu, S. Santoro, D. Sheinson, J. Hung, J.M. Giltnane, A.A. Pierce, K. Mesh, S. Lianoglou, J. Riegler, R.A.D. Carano, P. Eriksson, M. Höglund, L. Somarriba, D.L. Halligan, M.S. van der Heijden, Y. Loriot, J.E. Rosenberg, L. Fong, I. Mellman, D.S. Chen, M. Green, C. Derleth, G.D. Fine, P.S. Hegde, R.

Bourgon, T. Powles, TGFβ attenuates tumour response to PD-L1 blockade by contributing to exclusion of T cells, Nature, 554 (2018) 544–548.

22. W. Lin, X. Wang, Z. Wang, F. Shao, Y. Yang, Z. Cao, X. Feng, Y. Gao, J. He, Comprehensive Analysis Uncovers Prognostic and Immunogenic Characteristics of Cellular Senescence for Lung Adenocarcinoma, Frontiers in cell and developmental biology, 9 (2021) 780461.
23. J.N. Guo, D. Chen, S.H. Deng, J.R. Huang, J.X. Song, X.Y. Li, B.B. Cui, Y.L. Liu, Identification and quantification of immune infiltration landscape on therapy and prognosis in left- and right-sided colon cancer, Cancer immunology, immunotherapy: CII, 71 (2022) 1313–1330.
24. S. Wang, Y. Xiong, Q. Zhang, D. Su, C. Yu, Y. Cao, Y. Pan, Q. Lu, Y. Zuo, L. Yang, Clinical significance and immunogenomic landscape analyses of the immune cell signature based prognostic model for patients with breast cancer, Briefings in bioinformatics, 22 (2021).
25. X. Gu, J. Guan, J. Xu, Q. Zheng, C. Chen, Q. Yang, C. Huang, G. Wang, H. Zhou, Z. Chen, H. Zhu, Model based on five tumour immune microenvironment-related genes for predicting hepatocellular carcinoma immunotherapy outcomes, Journal of translational medicine, 19 (2021) 26.
26. X. Zhang, M. Shi, T. Chen, B. Zhang, Characterization of the Immune Cell Infiltration Landscape in Head and Neck Squamous Cell Carcinoma to Aid Immunotherapy, Molecular therapy. Nucleic acids, 22 (2020) 298–309.
27. J. Lamb, The Connectivity Map: a new tool for biomedical research, Nature reviews. Cancer, 7 (2007) 54–60.
28. F. Gaudreault, L.P. Morency, R.J. Najmanovich, NRGsuite: a PyMOL plugin to perform docking simulations in real time using FlexAID, Bioinformatics (Oxford, England), 31 (2015) 3856–3858.
29. Y. Zhang, J. Peng, H. Du, N. Zhang, X. Fang, Identification and Validation of Immune- and Stemness-Related Prognostic Signature of Melanoma, Frontiers in cell and developmental biology, 9 (2021) 755284.
30. Z. Wu, L. Chen, C. Jin, J. Xu, X. Zhang, Y. Yao, A novel pyroptosis-associated gene signature for immune status and prognosis of cutaneous melanoma, PeerJ, 9 (2021) e12304.
31. F. Zeng, J. Su, C. Peng, M. Liao, S. Zhao, Y. Guo, X. Chen, G. Deng, Prognostic Implications of Metabolism Related Gene Signature in Cutaneous Melanoma, Frontiers in oncology, 10 (2020) 1710.
32. J. Tian, C. Ma, L. Yang, Y. Sun, Y. Zhang, Prognostic Value and Immunological Characteristics of a Novel RNA Binding Protein Signature in Cutaneous Melanoma, Frontiers in genetics, 12 (2021) 723796.
33. M. Tian, J. Yang, J. Han, J. He, W. Liao, A novel immune checkpoint-related seven-gene signature for predicting prognosis and immunotherapy response in melanoma, International immunopharmacology, 87 (2020) 106821.
34. D. Landi, V. Moreno, E. Guino, P. Vodicka, B. Pardini, A. Naccarati, F. Canzian, R. Barale, F. Gemignani, S. Landi, Polymorphisms affecting micro-RNA regulation and associated with the risk of dietary-related cancers: a review from the literature and new evidence for a functional role of rs17281995

(CD86) and rs1051690 (INSR), previously associated with colorectal cancer, Mutation research, 717 (2011) 109–115.

35. A. Naimi, R.N. Mohammed, A. Raji, S. Chupradit, A.V. Yumashev, W. Suksatan, M.N. Shalaby, L. Thangavelu, S. Kamrava, N. Shomali, A.D. Sohrabi, A. Adili, A. Noroozi-Aghideh, E. Razeghian, Tumor immunotherapies by immune checkpoint inhibitors (ICIs); the pros and cons, Cell communication and signaling: CCS, 20 (2022) 44.
36. M.C. Kirchberger, S. Ugurel, J. Mangana, M.V. Heppt, T.K. Eigentler, C. Berking, D. Schadendorf, G. Schuler, R. Dummer, L. Heinzerling, MEK inhibition may increase survival of NRAS-mutated melanoma patients treated with checkpoint blockade: Results of a retrospective multicentre analysis of 364 patients, European journal of cancer (Oxford, England: 1990), 98 (2018) 10–16.
37. H. Liu, Z. Hu, H. Chen, Y. Yan, Z. Le, C. Wei, W. Cao, T. Chen, Y. Chen, L. Liu, Self-degradable poly(β-amino ester)s promote endosomal escape of antigen and agonist, Journal of controlled release: official journal of the Controlled Release Society, 345 (2022) 91–100.
38. C. Wang, J. Shi, J. Xu, Q. Fu, Y. Ding, J. Yang, B. Liu, Q. Gao, J. Qin, C. Liang, NLRC3 High Expression Represents a Novel Predictor for Positive Overall Survival Correlated With CCL5 and CXCL9 in HCC Patients, Frontiers in oncology, 12 (2022) 815326.
39. M.L. Carbone, G. Madonna, A. Capone, M. Bove, S. Mastroeni, L. Levati, M. Capone, P.A. Ascierto, F. De Galitiis, S. D'Atri, C. Fortes, E. Volpe, C.M. Failla, Vitiligo-specific soluble biomarkers as early indicators of response to immune checkpoint inhibitors in metastatic melanoma patients, Scientific reports, 12 (2022) 5448.
40. E.S. Borden, A.C. Adams, K.H. Buetow, M.A. Wilson, J.E. Bauman, C. Curiel-Lewandrowski, H.S. Chow, B.J. LaFleur, K.T. Hastings, Shared Gene Expression and Immune Pathway Changes Associated with Progression from Nevi to Melanoma, Cancers, 14 (2021).
41. J.L. Xu, Y. Guo, FCGR1A Serves as a Novel Biomarker and Correlates With Immune Infiltration in Four Cancer Types, Frontiers in molecular biosciences, 7 (2020) 581615.
42. C. Lu, J.D. Klement, A.D. Smith, D. Yang, J.L. Waller, D.D. Browning, D.H. Munn, K. Liu, p50 suppresses cytotoxic T lymphocyte effector function to regulate tumor immune escape and response to immunotherapy, Journal for immunotherapy of cancer, 8 (2020).
43. N.D. Marin, B.A. Krasnick, M. Becker-Hapak, L. Conant, S.P. Goedegebuure, M.M. Berrien-Elliott, K.J. Robbins, J.A. Foltz, M. Foster, P. Wong, C.C. Cubitt, J. Tran, C.B. Wetzel, M. Jacobs, A.Y. Zhou, D. Russler-Germain, L. Marsala, T. Schappe, R.C. Fields, T.A. Fehniger, Memory-like Differentiation Enhances NK Cell Responses to Melanoma, Clinical cancer research: an official journal of the American Association for Cancer Research, 27 (2021) 4859–4869.
44. C.B. Crayne, S. Albeituni, K.E. Nichols, R.Q. Cron, The Immunology of Macrophage Activation Syndrome, Frontiers in immunology, 10 (2019) 119.
45. H. Inoue, J.H. Park, K. Kiyotani, M. Zewde, A. Miyashita, M. Jinnin, Y. Kiniwa, R. Okuyama, R. Tanaka, Y. Fujisawa, H. Kato, A. Morita, J. Asai, N. Katoh, K. Yokota, M. Akiyama, H. Ihn, S. Fukushima, Y. Nakamura, Intratumoral expression levels of PD-L1, GZMA, and HLA-A along with oligoclonal T cell

expansion associate with response to nivolumab in metastatic melanoma, Oncoimmunology, 5 (2016) e1204507.

46. B. Rah, R.A. Rather, G.R. Bhat, A.B. Baba, I. Mushtaq, M. Farooq, T. Yousuf, S.B. Dar, S. Parveen, R. Hassan, F. Mohammad, I. Qassim, A. Bhat, S. Ali, M.H. Zargar, D. Afroze, JAK/STAT Signaling: Molecular Targets, Therapeutic Opportunities, and Limitations of Targeted Inhibitions in Solid Malignancies, Frontiers in pharmacology, 13 (2022) 821344.
47. F. Erdogan, T.B. Radu, A. Orlova, A.K. Qadree, E.D. de Araujo, J. Israelian, P. Valent, S.M. Mustjoki, M. Herling, R. Moriggl, P.T. Gunning, JAK-STAT core cancer pathway: An integrative cancer interactome analysis, Journal of cellular and molecular medicine, 26 (2022) 2049–2062.
48. M. Fojtova, V. Boudny, A. Kovarik, L. Lauerova, L. Adamkova, K. Souckova, J. Jarkovsky, J. Kovarik, Development of IFN-gamma resistance is associated with attenuation of SOCS genes induction and constitutive expression of SOCS 3 in melanoma cells, British journal of cancer, 97 (2007) 231–237.
49. X. Li, X. Sun, X. Guo, X. Li, S. Peng, X. Mu, Chemical reagents modulate nucleic acid-activated toll-like receptors, Biomedicine & pharmacotherapy = Biomedecine & pharmacotherapie, 147 (2022) 112622.
50. T. Tsubata, Role of inhibitory B cell co-receptors in B cell self-tolerance to non-protein antigens, Immunological reviews, 307 (2022) 53–65.
51. S. Ren, X. Wang, G. Jin, Conjugate of ibrutinib with a TLR7 agonist suppresses melanoma progression and enhances antitumor immunity, International journal of biological sciences, 18 (2022) 166–179.
52. X. Lei, Y. Lei, J.K. Li, W.X. Du, R.G. Li, J. Yang, J. Li, F. Li, H.B. Tan, Immune cells within the tumor microenvironment: Biological functions and roles in cancer immunotherapy, Cancer letters, 470 (2020) 126–133.
53. K.E. Pauken, E.J. Wherry, SnapShot: T Cell Exhaustion, Cell, 163 (2015) 1038–1038.e1031.
54. N.S. Butler, J.C. Nolz, J.T. Harty, Immunologic considerations for generating memory CD8 T cells through vaccination, Cellular microbiology, 13 (2011) 925–933.
55. D.M. Pardoll, S.L. Topalian, The role of CD4 + T cell responses in antitumor immunity, Current opinion in immunology, 10 (1998) 588–594.
56. H. Zhao, L. Wu, G. Yan, Y. Chen, M. Zhou, Y. Wu, Y. Li, Inflammation and tumor progression: signaling pathways and targeted intervention, Signal transduction and targeted therapy, 6 (2021) 263.
57. D.I. Gabrilovich, Myeloid-Derived Suppressor Cells, Cancer immunology research, 5 (2017) 3–8.
58. M.R. Galdiero, G. Marone, A. Mantovani, Cancer Inflammation and Cytokines, Cold Spring Harbor perspectives in biology, 10 (2018).
59. F.J. Lowery, S. Krishna, R. Yossef, N.B. Parikh, P.D. Chatani, N. Zacharakis, M.R. Parkhurst, N. Levin, S. Sindiri, A. Sachs, K.J. Hitscherich, Z. Yu, N.R. Vale, Y.C. Lu, Z. Zheng, L. Jia, J.J. Gartner, V.K. Hill, A.R. Copeland, S.K. Nah, R.V. Masi, B. Gasmi, S. Kivitz, B.C. Paria, M. Florentin, S.P. Kim, K.I. Hanada, Y.F. Li, L.T. Ngo, S. Ray, M.L. Shindorf, S.T. Levi, R. Shepherd, C. Toy, A.Y. Parikh, T.D. Prickett, M.C. Kelly, R. Beyer, S.L. Goff, J.C. Yang, P.F. Robbins, S.A. Rosenberg, Molecular signatures of antitumor

neoantigen-reactive T cells from metastatic human cancers, Science (New York, N.Y.), 375 (2022) 877–884.

60. B.E. Brito, M.A. García, Y.M. De Gouveia, P. Bolaños, S. Devis, G. Bernal, V.A. Tortorici-Brito, L. Baute, G. Díaz-Serrano, V. Tortorici, Concomitant Antihyperalgesic and Antitumor Effects of Gabapentin in a Murine Cancer Pain Model, International journal of molecular sciences, 22 (2021).
61. S. Liu, S. Miriyala, M.A. Keaton, C.T. Jordan, C. Wiedl, D.K. Clair, J.A. Moscow, Metabolic effects of acute thiamine depletion are reversed by rapamycin in breast and leukemia cells, PloS one, 9 (2014) e85702.

Figures

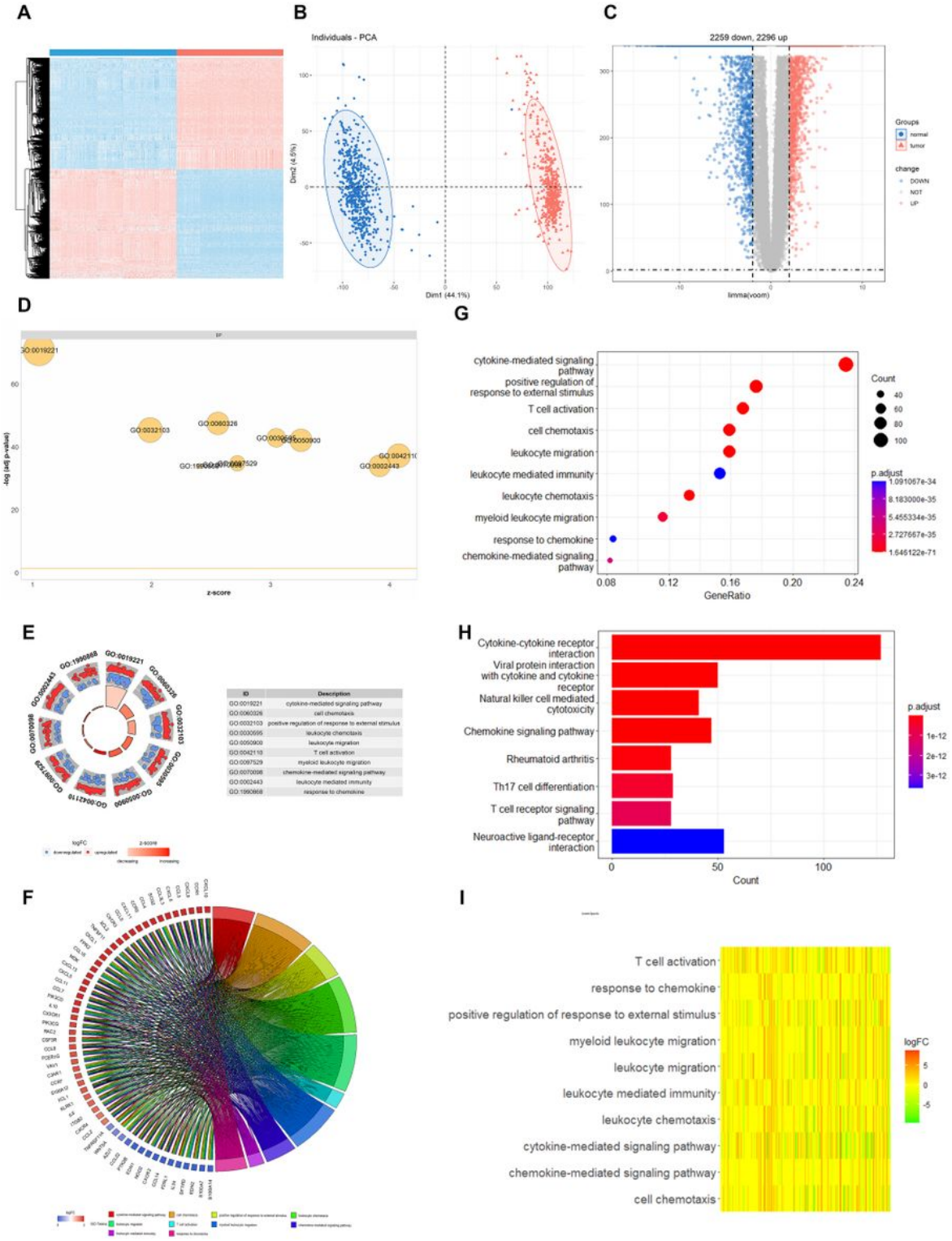

Figure 1

Difference of genomic landscape between normal and cutaneous melanoma. (A) Hierarchical clustering of differentially expressed genes between normal and cutaneous melanoma samples. Red represents up-regulated and blue represents down-regulated. (B) PCA visualization of differentially expressed genes. (C)Volcano plot of differentially expressed genes. (D) Biological processes enrichment of gene ontology functional enrichment. (E) Molecular function enrichment of gene ontology functional enrichment. (F)

Chord plot of gene ontology functional enrichment. The left half-circle indicates that the genes are sorted by |logFC| and the right half-circle indicates that the gene ontology enrichment analysis term is sorted by strong and weak variation. Red represents up-regulation and blue represents down-regulation, and color shades represent fold change. (G) Cellular component enrichment of gene ontology functional enrichment. (H) KEGG pathway enrichment analyses for differentially expressed genes. All enriched pathways were significant and the color depth represented enriched adjusted *P* value. (I) Heatmap of differentially expressed genes between normal and cutaneous melanoma samples. Different colors represent different interaction strength relationships.

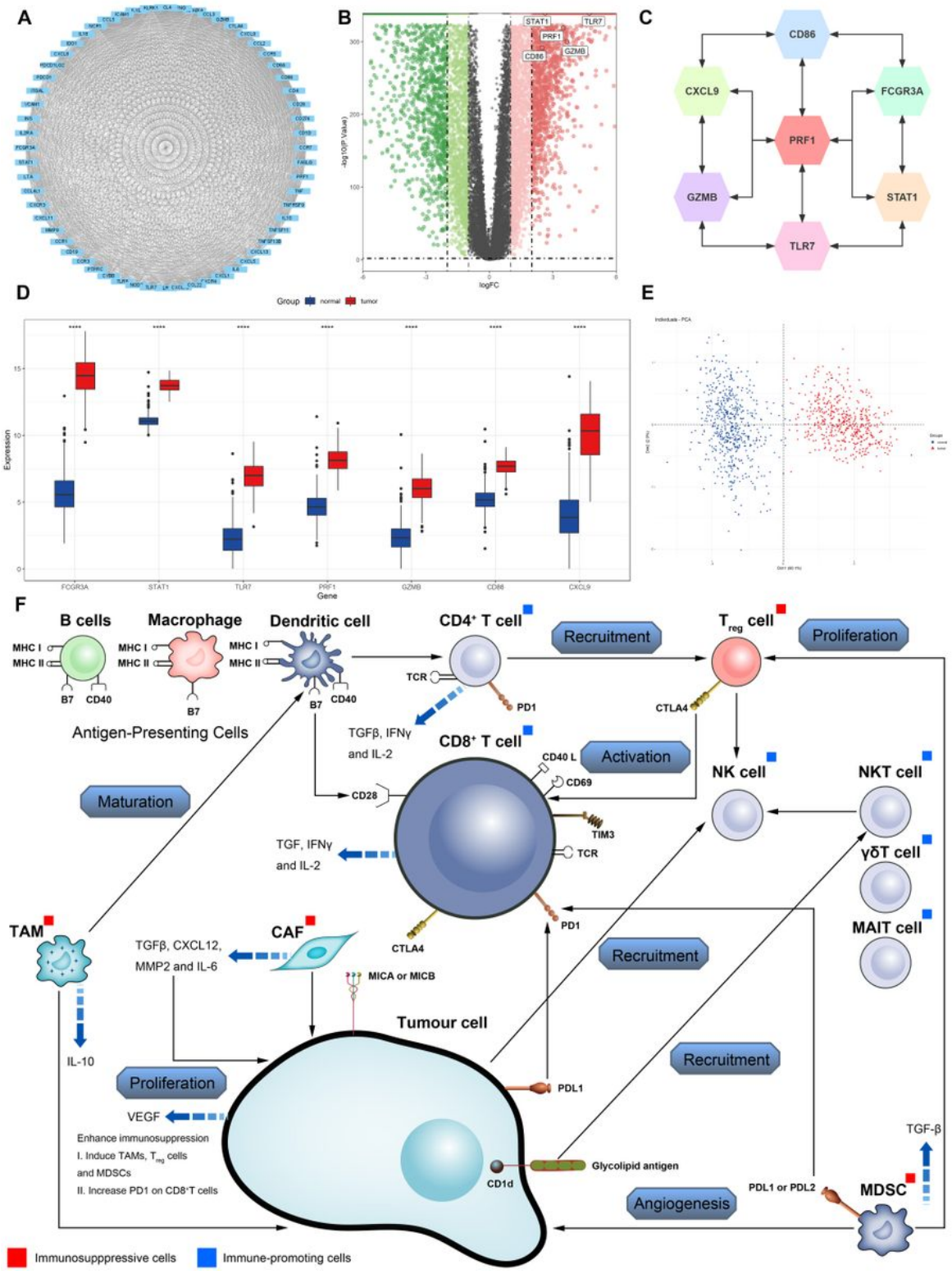

Figure 2

Identification of key molecules in cutaneous melanoma. (A) Construction of protein-protein interaction (PPI) network among differentially expressed genes. (B) Volcano plot constructed with the cut-off criterion $P<0.05$ and $|logFC|\geq 1$. (C) The relationship among the seven key molecules at the protein level, each gene is closely linked to each other at the protein level. (D) The seven key molecules expressed in the normal skin and cutaneous melanoma (*$P<0.05$, **$P<0.01$, ***$P<0.001$, ****$P<0.0001$). (E) Principal

component analysis for the key molecules revealed. This result shows that seven key molecules can distinguish very well between normal skin and cutaneous melanoma. (F) Effect of immune and stromal cells on cutaneous melanoma.

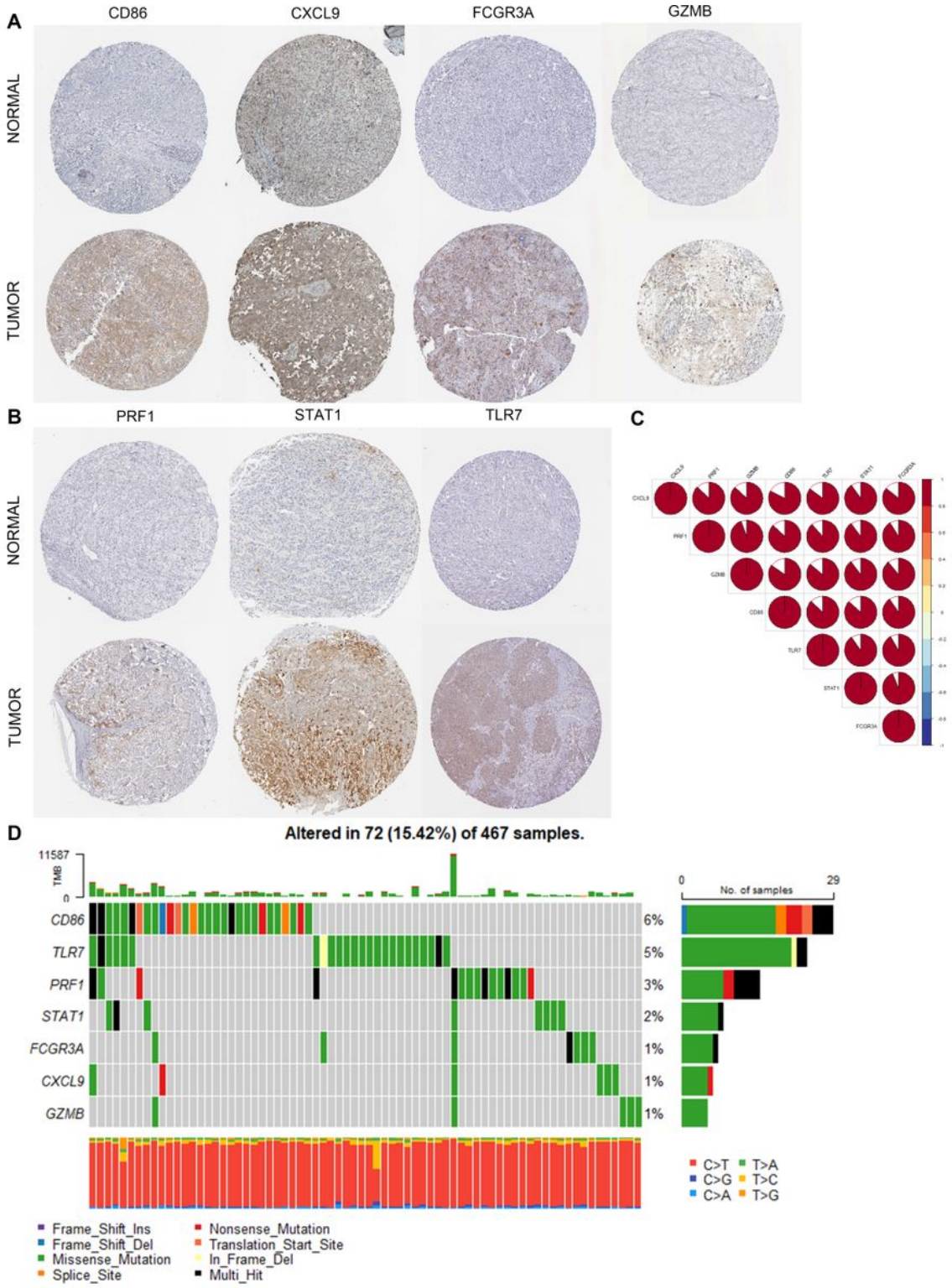

Figure 3

Multi-omics analysis of identified seven key molecules. (A-B) The immunohistochemical staining results revealed significant differences of key molecules (CD86, CXCL9, FCRG3A, GZMB, PRF1, STAT1, TLR7) at the protein expression between normal skin and cutaneous melanoma obtained at the Human Proteins Atlas. (C) The correlation between the seven key molecules using spearman analysis. The color area represents the magnitude of correlation intensity, red represents positive correlation and blue represents negative correlation. The key molecules in the figure show very good correlation with each other. (D) Mutation landscape of seven key molecules in 467 samples of TCGA cohort. Different color modules represent different molecular mutation frequencies.

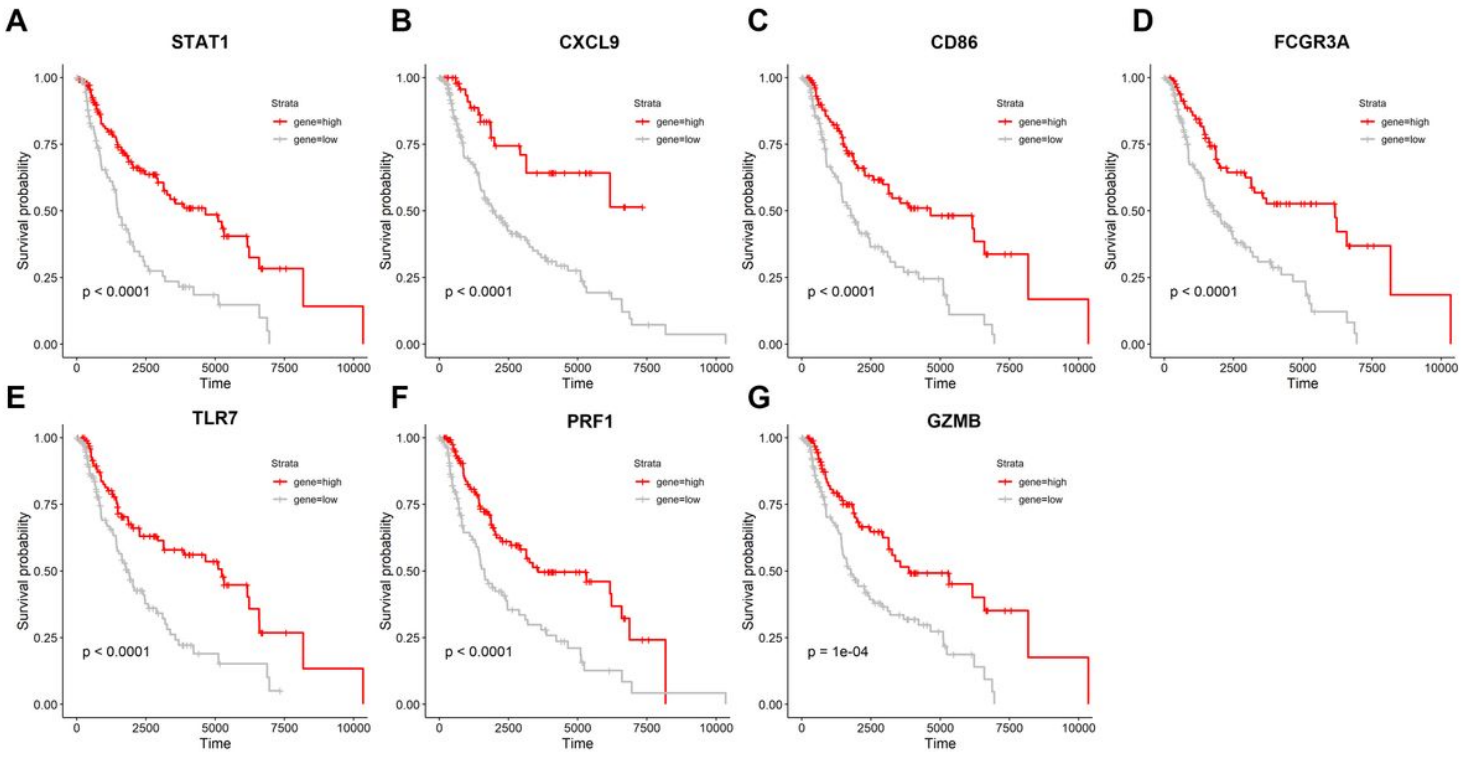

Figure 4

Seven Kaplan-Meier curves are based on samples from the GTEX and TCGA databases, extracting data from these seven genes and combining them with survival times. The sample size is 1025. (A-G) Survival analysis for seven key molecules. Seven key molecules which includes STAT1, CXCL9, CD86, FCGR3A, TLR7, PRF1, GZMB.

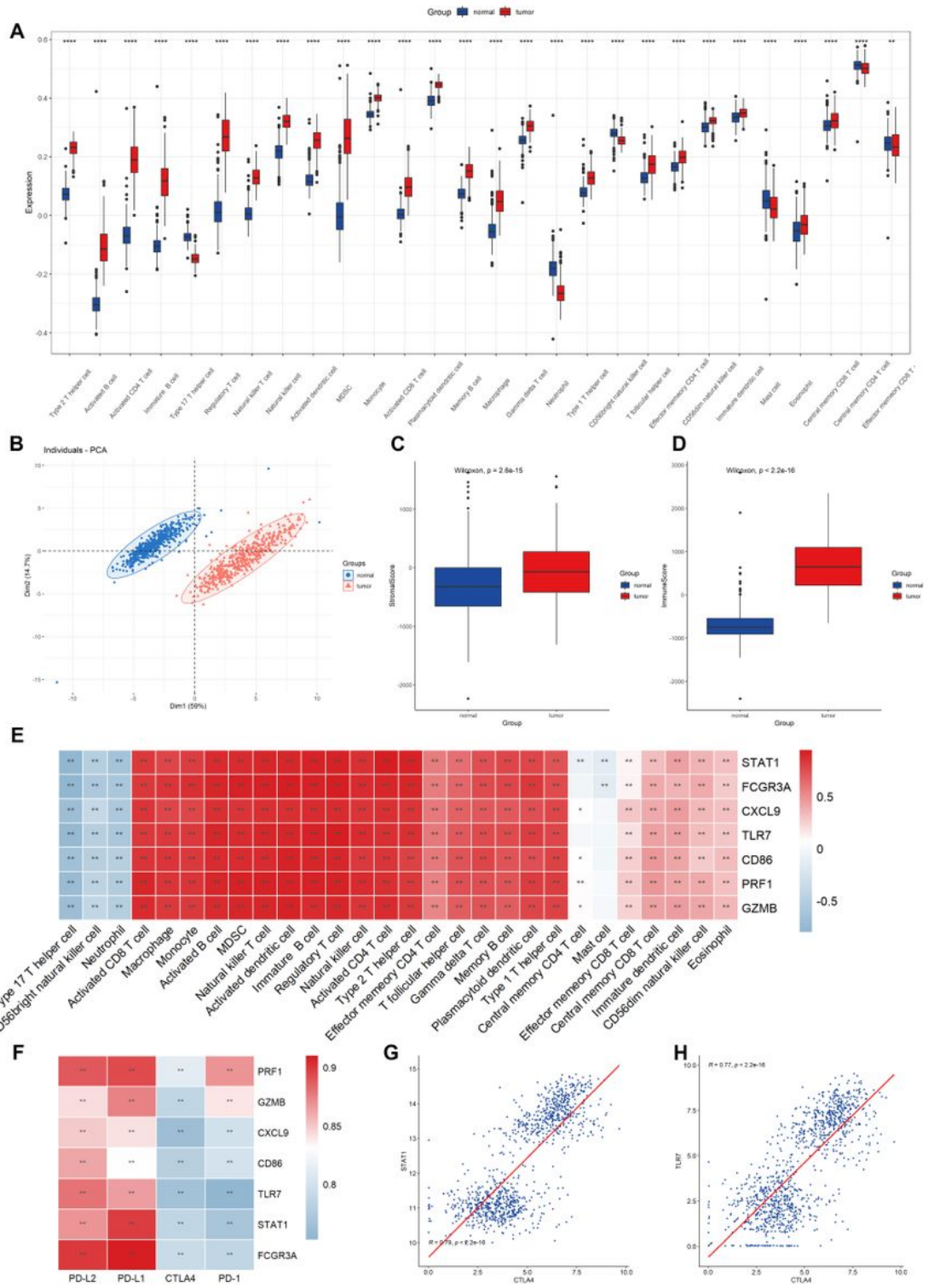

Figure 5

Evaluation of 28 TME immune cell infiltration characterization. (A) Differences in 28 TME infiltration cells between normal skin and cutaneous melanoma (*P<0.05, **P<0.01, ***P<0.001, ****P<0.0001). The results showed that all immune cells were significantly different between the two types of samples. (B) Principal component analysis. The results demonstrated that the two separate taxa, suggesting there existed significantly differences in the landscape of 28 TME immune cell infiltration between normal skin

and cutaneous melanoma. (C) Difference in StromalScore between normal and tumor tissues using ESTIMATE algorithm. (D) Difference in ImmuneScore between normal and tumor tissues using ESTIMATE algorithm. (E) The correlation between seven key molecule and each TME infiltration cell type. The results showed a strong correlation between them, red represents positive and blue represents negative. (F) The correlation between the seven key molecules and four immune checkpoint molecules. The results demonstrated a strong correlation between them. (G) The correlation between STAT1 expression and CTLA4 expression. (H) The correlation between TLR7 expression and CTLA4 expression.

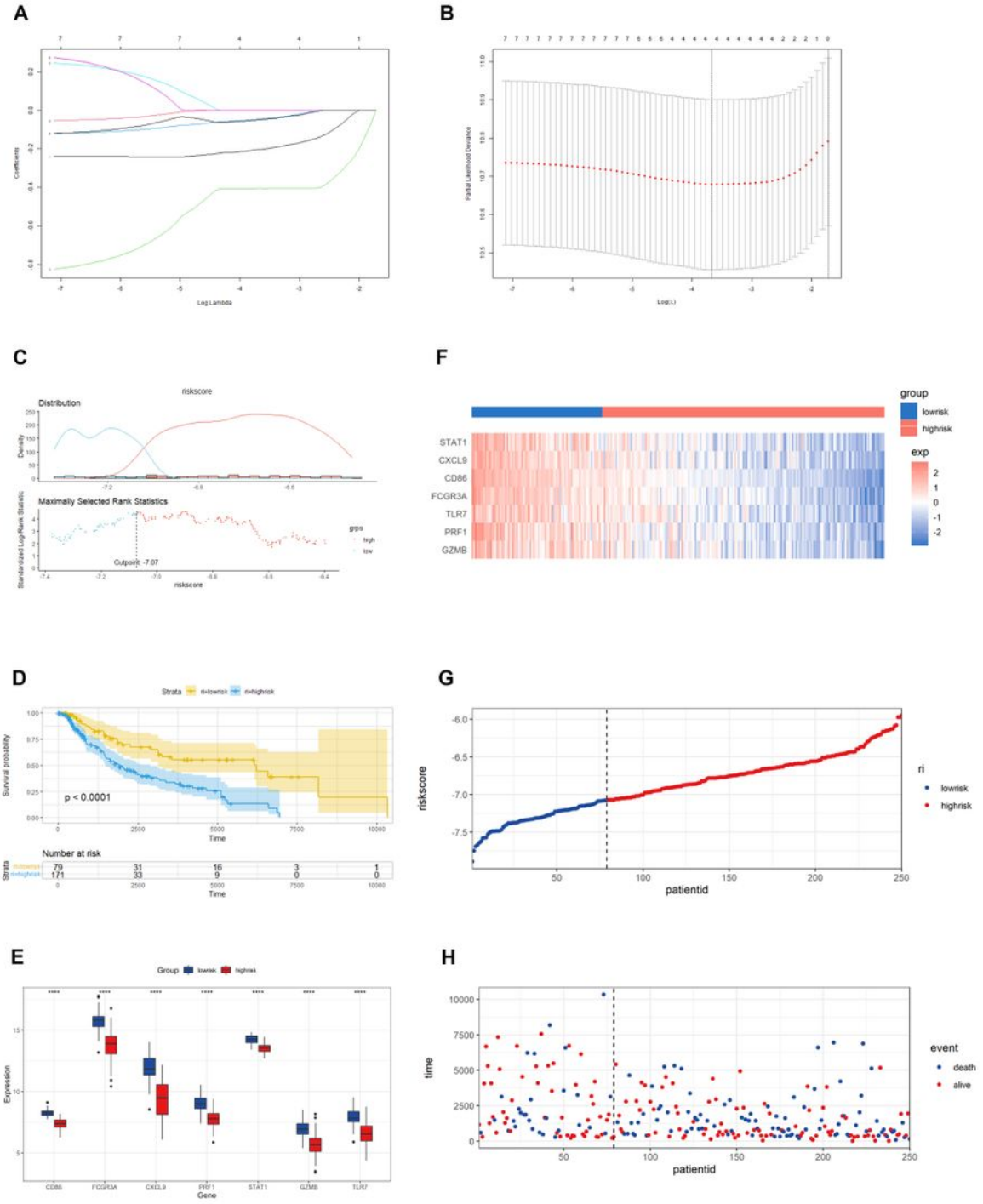

Figure 6

Construction of riskScore signature in cutaneous melanoma. (A) Least absolute shrinkage and selection operator (LASSO) coefficient profiles of the seven key molecules. Horizontal axis represents log of independent variable λ. Vertical axis represents coefficient of independent variable. (B) Tenfold cross-validation of tuning parameters in LASSO model. (C) The optimal cut-off point to dichotomize riskScore into low and high groups was determined by MaxStat R package. The optimal cutoff point was -7.07. (D) Survival analyses for low (79 samples) and high (171 samples) riskScore groups using Kaplan-Meier curves. (E) The seven key molecules expressed in the low and high risk groups (*P<0.05, **P <0.01, ***P <0.001, ****P <0.0001). The results showed that a strongly significant difference was exhibited between the groups. (F) The median value and distribution of the risk score. (G) The distribution of overall survival (OS) status. (H) Hierarchical clustering of seven key genes between low and high risk groups. Red represents up-regulated and blue represents down-regulated.

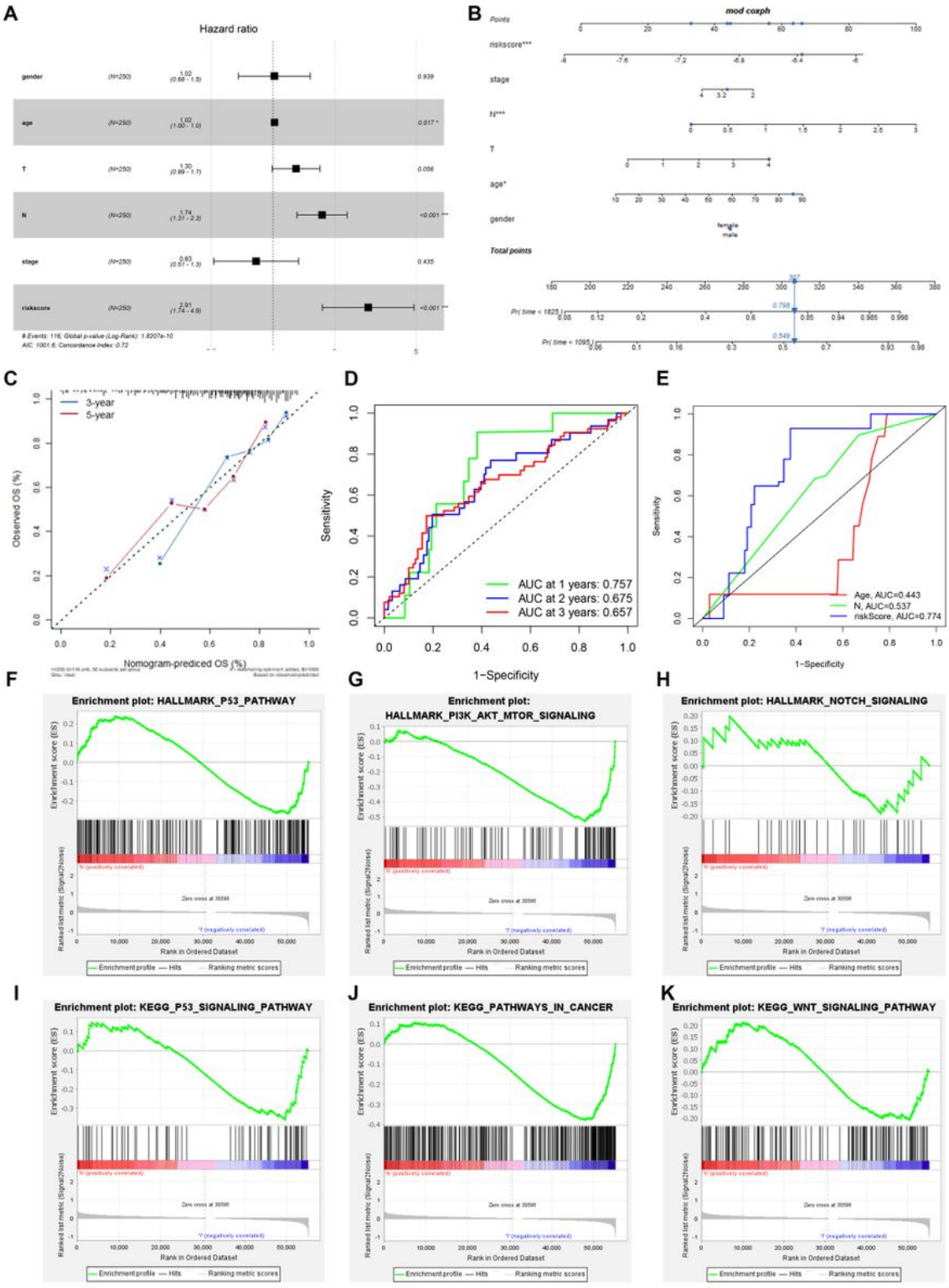

Figure 7

Prognostic value of the riskScore gene signature in cutaneous melanoma. (A) Forest plot. The results demonstrated that the riskScore and N were independent prognostic biomarkers using multivariate analyses. (B) The nomogram, including clinical features and the risk score, for predicting outcomes in patients. (C) The calibration curve analysis showed that the actual and the predicted 1-, 3-, 5-year survival times were consistent compared with the reference line (the 45-degree line). (D) The receiver operating

characteristic curve (ROC) analysis of risk scores based on 1-, 2-, and 3-year OS in TCGA group. (E) The receiver operating characteristic curve (ROC) analysis of risk scores and other clinical characteristics based on OS in TCGA group. (F-K) The GSEA enrichment reveal several significant signaling pathways. (F) HALLMARK P53 pathway. (G) HALLMARK PI3K AKT MTOR signaling pathway. (H) HALLMARK NOTCH signaling pathway. (I) KEGG P53 pathway. (J) KEGG pathway in cancer. (L) KEGG WNT signaling pathway.

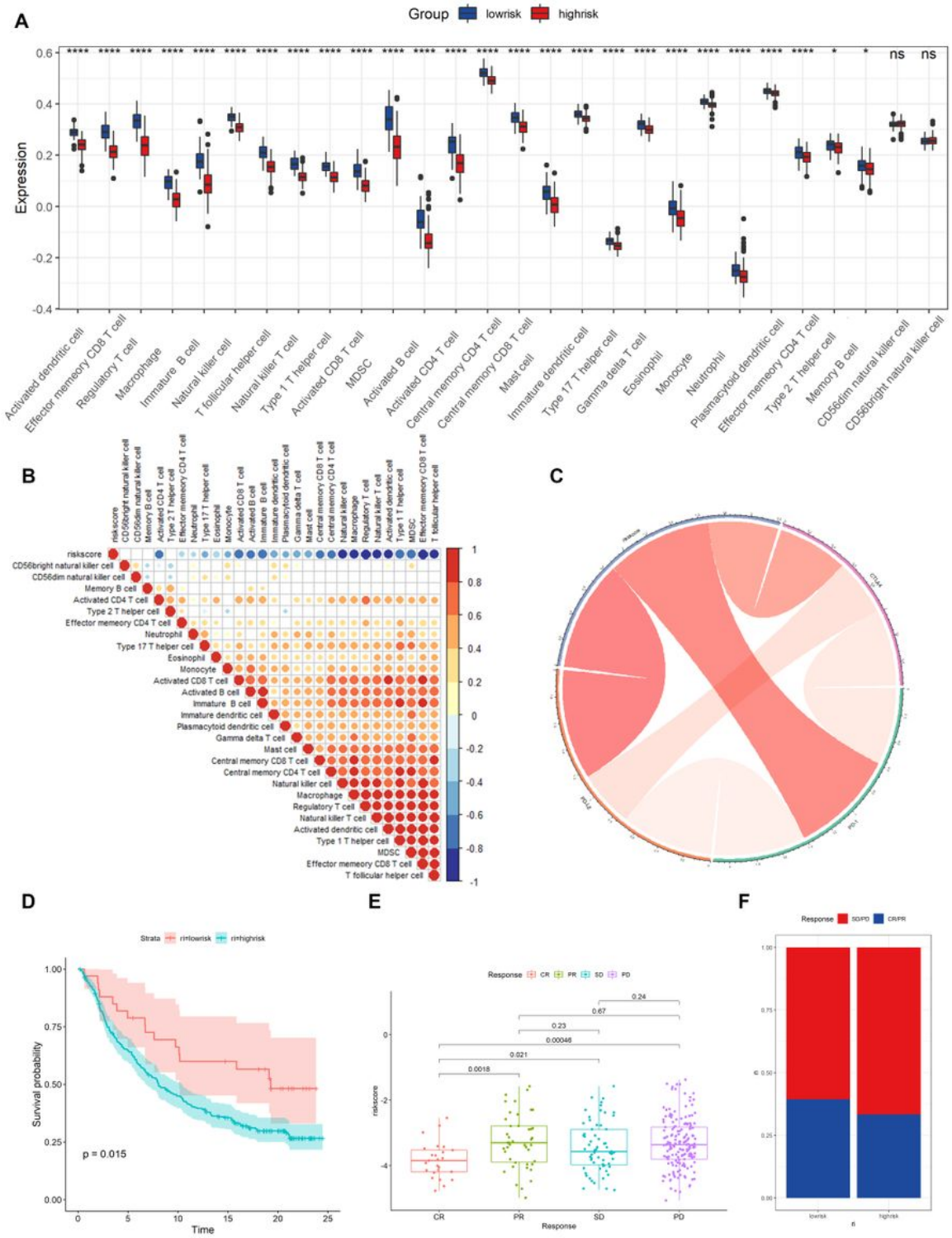

Figure 8

The role of riskScore signature in the TME cell infiltration and immunotherapeutic responses. (A) Differences in 28 TME infiltration cells between low and high risk groups (*P<0.05, **P <0.01, ***P <0.001, ****P <0.0001). The results demonstrated that most TME cells (26 types) exist significant differences. (B) The correlation between riskScore signature and 28 TME cell infiltration. Color shades represent the strength of the association, blue represents negative correlation and red represents positive correlation. (C) The correlation between riskScore signature and immune checkpoint molecules. Blue represents negative correlation and red represents positive correlation. (D) Survival analyses for high and low risk score groups in anti-PD-L1 immunotherapy cohort using Kaplan-Meier curves. (E) The difference of riskScore in different anti-PD-L1 clinical response groups. CR, complete response. PD, progressive disease. PR, partial response. SD, stable disease. (F) The proportion of patients with response to PD-L1 blockade therapy in high or low riskScore groups.

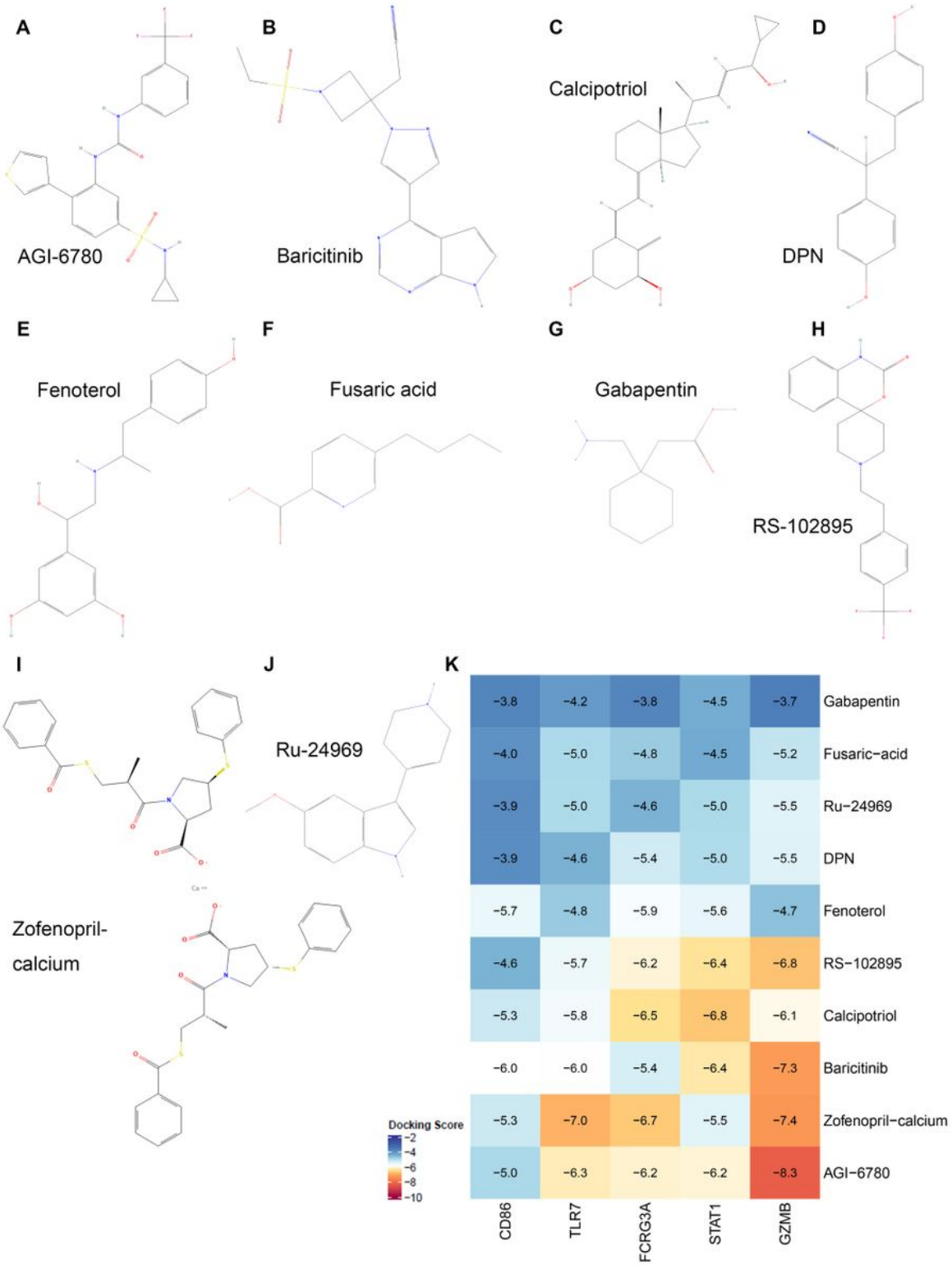

Figure 9

Chemical structure depiction of the top ten most significant drugs. (A) AGI-6780. (B) Baricitinib. (C) Calcipotriol. (D) DPN. (E) Fenoterol. (F) Fusaric acid. (G) Gabapentin. (H) RS-102895. (I) Zofenopril calcium. (J) Ru-24969. (K) Heat map of the lowest binding energy for molecular docking.

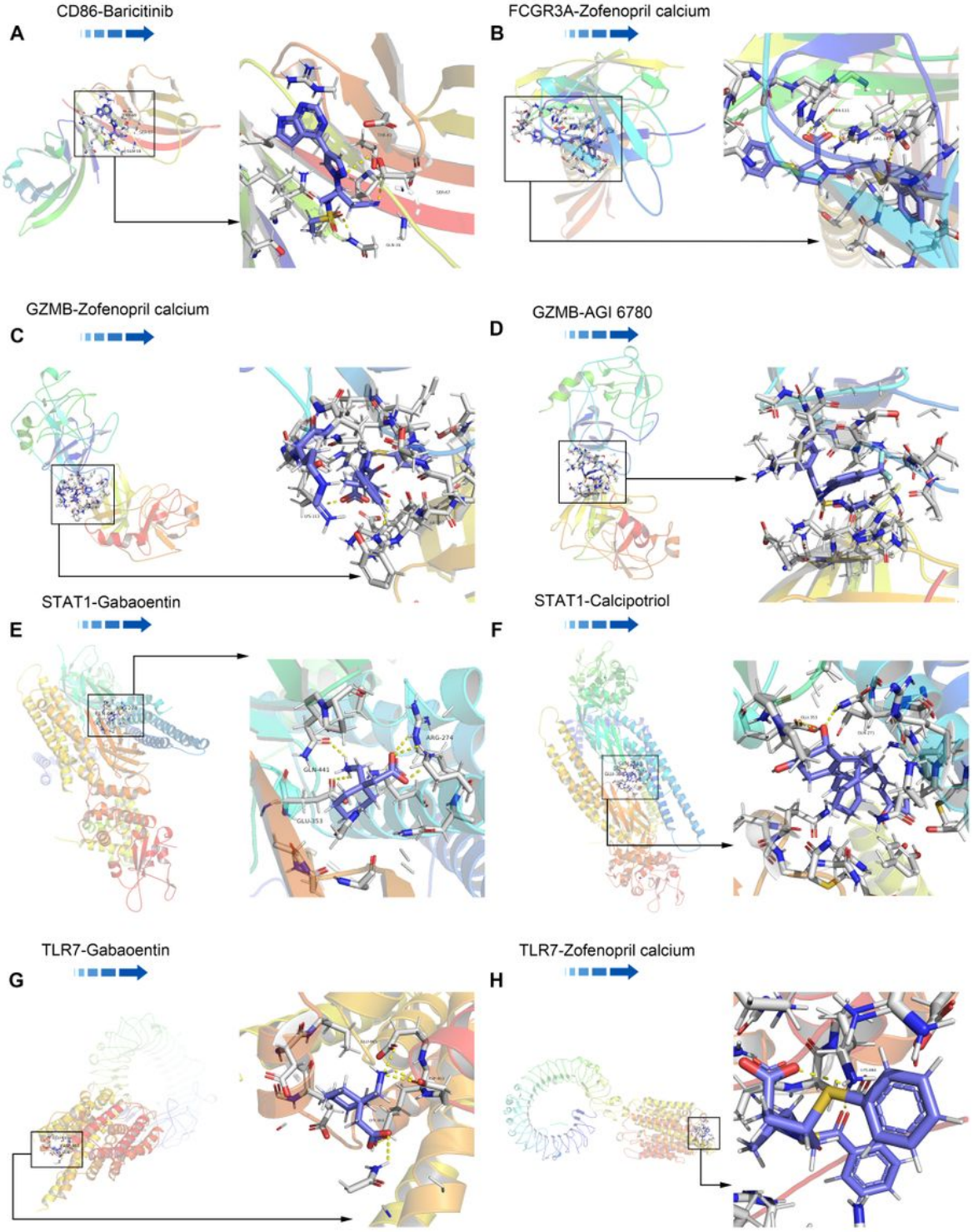

Figure 10

Docking diagram of small molecular drugs with targets. (A) CD86-Baricitinib. (B) FCGR3A-Zofenopril calcium. (C) GZMB-Zofenopril calcium. (D) GZMB-AGI 6780. (E) STAT1-Gabaoentin. (F) TLR7-Gabaoentin. (G) STAT1-Calcipotriol. (H) TLR7-Zofenopril calcium.

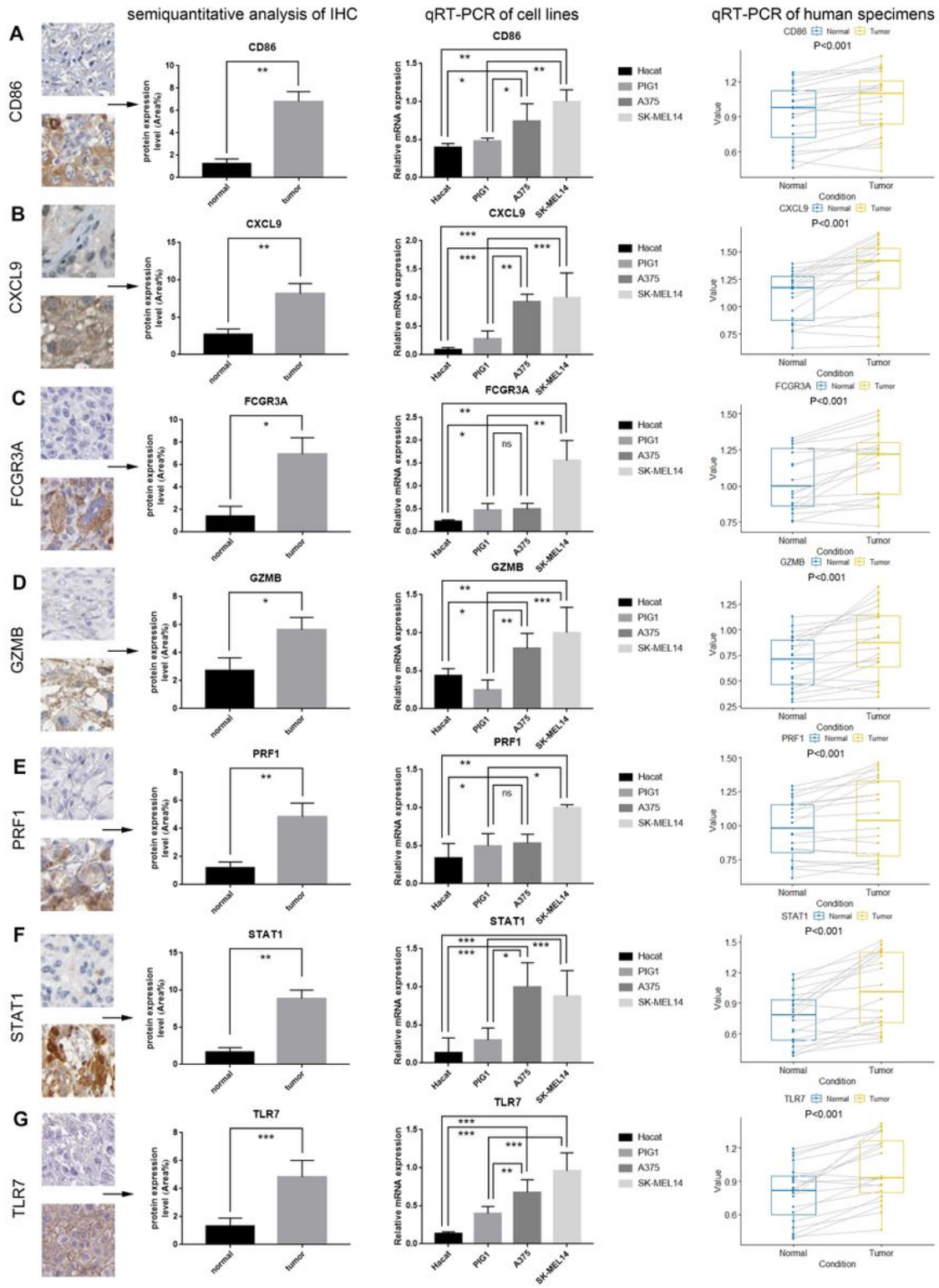

Figure 11

Validation of the mRNA and protein expression of seven key genes. Results of the first column represents the semiquantitative analysis results which obtained from the IHC results downloaded from the human protein atlas (see Figure 3 for a complete view of the immunohistochemistry images). Results of the second column represents the qRT-PCR results from four cell lines (Hacat, PIG1, A375 and SK-MEL 14). Results of the third column represents the qRT-PCR results of tissue specimens from 20 patients, which

taken from normal skin and cutaneous melanoma. (A-G) represents the results of seven key genes, including CD86, CXCL9, FCGR3A, GZMB, PRF1, STAT1, TLR7 (ns, not significant, *P<0.05, **P <0.01, ***P <0.001).

Supplementary Files

This is a list of supplementary files associated with this preprint. Click to download.

- SupplementaryTable.docx
- Supplementaryfigure1.jpg
- Supplementaryfigure2.jpg